Chemical Engineering Journal 158 (2010) 51–60

Contents lists available at ScienceDirect

Chemical Engineering Journal

journal homepage: www.elsevier.com/locate/cej

Liquor flow in a model kraft batch digester

Quak Foo Lee, Chad P.J. Bennington*

Department of Chemical and Biological Engineering, University of British Columbia, 2360 East Mall, Vancouver, BC V6T 1Z3, Canada

ARTICLE INFO

Article history:
Received 7 April 2008
Received in revised form 15 August 2008
Accepted 18 August 2008

Keywords:
Kraft pulping
Batch digesters
Electrical resistance tomography
Liquor flow uniformity
Computational modelling

ABSTRACT

Batch digesters are solid–liquid reactors used to produce chemical pulp from wood chips. The literature shows that the extent of reaction (delignification) varies as a function of chip location in the vessel, with the extent of non-uniformity commonly attributed to poor and/or non-uniform liquor flow through the digester (which causes poor chemical and heat distribution through the chip mass during the cook). Electrical resistance tomography (ERT) was used to evaluate the uniformity of liquor flow in a laboratory scale-model digester (a 1:15 geometrically scaled vessel) with model particles used in place of wood chips (the vessel to particle diameter ratio was 93:1 to minimize wall effects) and close approximation of the liquor superficial velocity and pore Reynolds number. Local flow velocities were also measured for common flow conditions using ERT data and pixel–pixel cross-correlation techniques, with the results compared with computational simulations made using a commercial CFD code.

The tomographic data shows that it is possible to create uniform zones in the digester, although a stagnation point exists in the centre of the vessel at the screen level. This point coincides with the location of highest kappa numbers (the lowest extent of reaction) reported in industrial tests. Within the resolution of the tomographic technique local axial flow velocities were found to agree with calculated and computational results. The flow velocity data were used as input to a two-dimensional, mathematical model of reaction within the digester, with the variability of lignin distribution compared to available industrial data.

1. Introduction

Roughly 40% of the 188 million tonnes of kraft pulp produced world-wide each year is manufactured using batch digesters. These are chemical reactors which delignify wood chips using an aqueous solution of NaOH and Na_2S (called white liquor) at temperatures between 160 and 175 °C for periods approaching 2 h. The vessels are cylindrical, 2.5–5 m in diameter, 8.5–19 m in height and have volumes ranging from 70 to 400 m^3. Many digesters have a conical section at the base of the cylinder (comprising 6–10% of the total volume) to improve chip/pulp discharge following the cook.

In forced circulation digesters, cooking liquor is circulated through the vessel to ensure uniform heating of the chips at the beginning of the cook and continued mass transfer until the desired endpoint is reached. One common operational mode is to circulate liquor to both the top and bottom of the vessel and remove it through a set of extraction screens located just below the vessel midpoint. The extracted liquor is passed through an indirect steam heater and then returned to the digester. In some digesters, no effort is made to control the volume of liquor re-circulated to the top and bottom of the digester. In others, flow valves are used to control the liquor split, often with flow divided equally between the top and bottom circulation loops. However, the liquor split can be varied, and one strategy is to vary the flow ratio based on the volume of the chip bed above and below the extraction screens. During the cooking cycle, liquor circulation decreases as the chips are delignified and become more conformable and compacted which increases fluid flow resistance by decreasing the void fraction of the chip bed.

Pulp produced from batch digester operations is typically non-uniform, with the coefficient-of-variation (CoV) of kappa measurements ranging from 5 to 16% [1]. Chips located in the centre of the vessel at the level of the extraction screens were found to have the lowest degree of cooking/reaction (the highest kappa numbers) while chips below the screen level experienced the greatest extent of cooking. This variability was attributed to poor or non-uniform liquor flow through the vessel which allowed chemical and temperature variations to develop through the chip mass. To achieve uniform pulping liquor flow must ensure that each chip experiences the same time–temperature and time–concentration history.

Improving the uniformity of pulp produced during batch operations is an important goal for digester optimization and can lead to shorter cooking times (increased production), improved process stability and controllability, lower bleaching chemical usage in subsequent stages (which leads to improved environmental

* Corresponding author.
E-mail address: cpjb@chml.ubc.ca (C.P.J. Bennington).

1385-8947/$ – see front matter © 2008 Elsevier B.V. All rights reserved.
doi:10.1016/j.cej.2008.08.042

Nomenclature

d_p	particle equivalent diameter (mm)
D	diameter of column (m)
H	height of particles column (m)
L	length of column (m)
Q	flowrate (L/min)
u_s	fluid superficial velocity (mm/s)
z	distance in axial direction (m)

Subscripts

s	superficial
T	top
B	bottom
1	industrial scale
2	laboratory scale

Greek letters

κ	kappa number

performance), and improved pulp uniformity and strength. In this work, we use electrical resistance tomography (ERT) to evaluate the uniformity of zones created by the liquid phase and the local liquid axial velocity in a laboratory scale-model digester operated in batch mode. The data were used to rationalize measurements of pulp uniformity available in the literature and to provide input to a computational model that calculates the spatial distribution of reaction in the digester.

2. Experimental methods

A 30 L geometrically scaled model batch digester (1:15 scale) was fabricated from Plexiglas based on typical industrial designs (Fig. 1). The bottom of the vessel, below the screen level, was tapered at an angle of 60° (from the horizontal) to give a conical section comprising 11% of the vessel volume. The experimental apparatus allowed liquor (brine solutions) to be circulated through the vessel in a number of flow configurations, including the typical industrial configuration where liquor is added to both the top and bottom of the vessel and extracted from the screen section.

Two criteria were used to scale the tests: geometry ($L_1/D_1 = L_2/D_2$) and superficial velocity ($u_{s,1} = u_{s,2}$: proportional to the interstitial velocity ratio) where the indices refer to the industrial and laboratory-scale vessels. The chips of industrial digesters were modelled using incompressible disk-shaped high-density polyethylene (HDPE) pellets having a width of 4.6 ± 0.1 mm and a thickness of 2.0 ± 0.1 mm. These mono-disperse particles gave a bed voidage of 0.35, comparable to voidage estimates for chip beds during a cook (0.30–0.35). The vessel-to-particle diameter ratio for the laboratory vessel was $D/d_p = 93$ compared to $D/d_p = 583$ for an industrial digester. This implies that the wall-affected zone in the model digester, although minimized, occupies a greater fraction of the cross-sectional area than in industrial units. Liquid flow through the scaled vessel was in the laminar regime, as in industrial units. This was achieved by matching the superficial velocity in the model digester and ensuring that the pore Reynolds number calculated at the laboratory and industrial scales was in the laminar regime. Further details on the experimental design can be found in Lee and Bennington [2].

To image liquor flows, a P2000 electrical resistance tomography (ERT) unit (ITS, Manchester, UK) was used. Liquor streams having different conductivities (established using saline solutions of specific concentrations) were imaged as they moved through the model digester. Eight sensor planes were spaced at 7.5 cm intervals along the vessel axis, with each image plane consisting of 16 electrodes located at 22.5° intervals around the vessel periphery. The bottom three sensor planes were located in the conical section of the digester (from $z/H = 0.08$–0.28). In the upper section, sampling planes were located at $z/H = 0.47$–0.66. Circular electrodes were fabricated from stainless steel, with the electrode to column diameter ratio maintained at 0.078 ± 0.001. Electrodes were placed perpendicular to the vessel surface. The linear back projection (LBP) algorithm was used for image reconstruction with the gain map obtained from the smallest diameter plane (plane 1). Two-dimensional images from each plane were combined to yield pseudo three-dimensional representations of the flow.

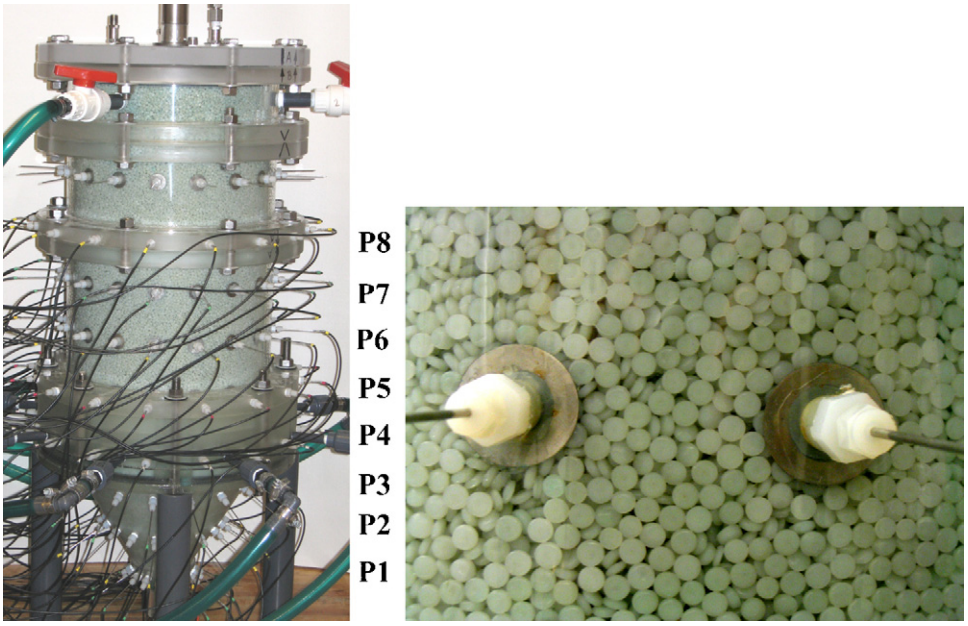

Fig. 1. Scale-model batch digester showing ERT imaging planes (left). Close up of ellipsoidal HDPE pellets ($d_p = 3.2$ mm, Sauter mean diameter) to model the solid phase. ERT sensor electrodes ($d = 2.2$ cm) are visible (right).

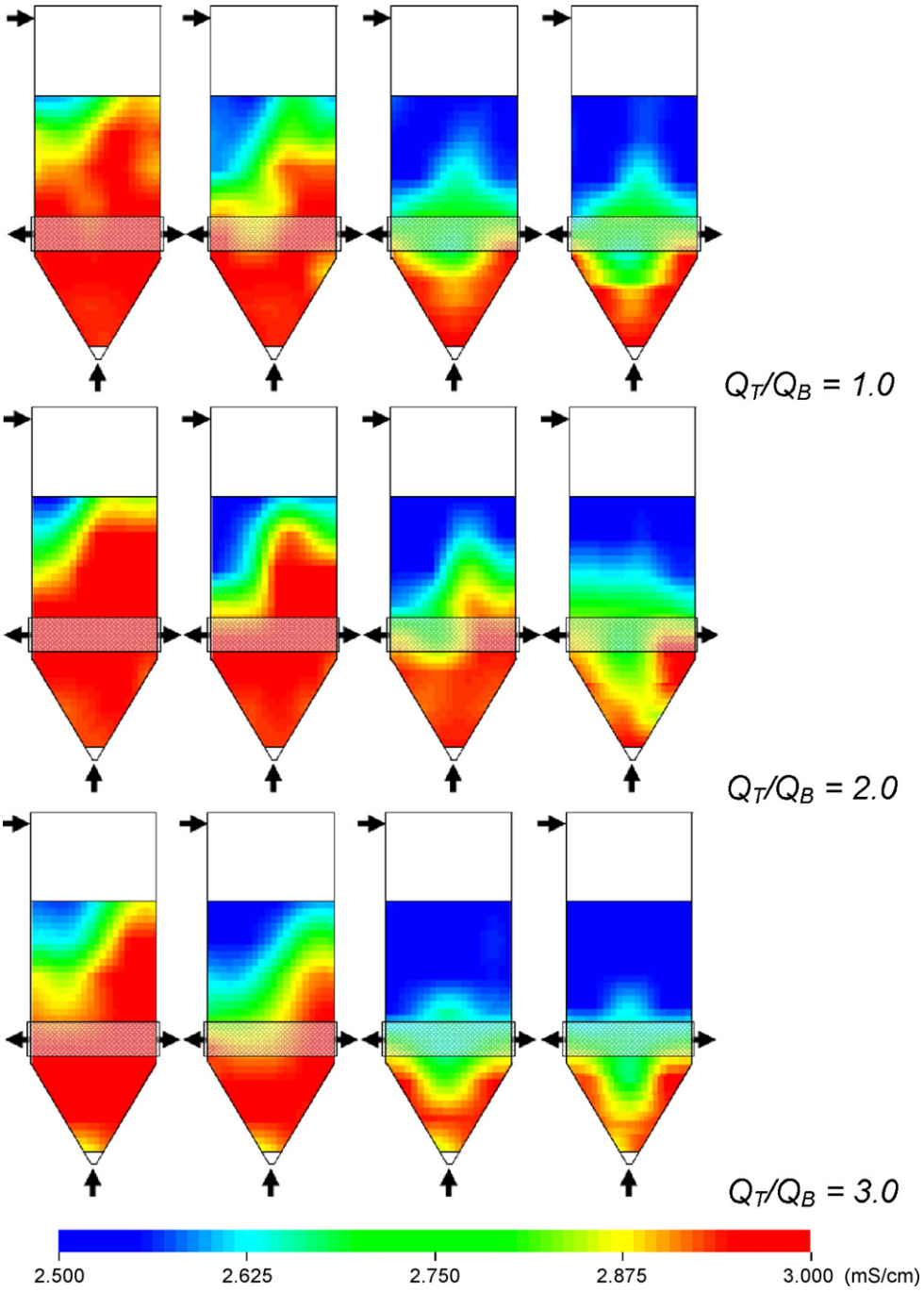

Fig. 2. Tomographic image reconstruction in the axial plane showing movement through the vessel as a function of time for a lower conductivity tracer (blue) added to the top circulation loop (Images are given at t = 25, 40, 88, 309 s from the time of tracer injection, from left to right). Q_T/Q_B = 1.0, 2.0 and 3.0 with Q_T = 12 L/min in all cases.

Tests were conducted to cover the range of typical industrial flows, specified as Q_T/Q_B (the liquor volumetric flow ratio between the top and bottom of the digester). A range of values were explored, from 0.5 to 3.0. The flow rate in each section of the digesters ranged from 4 to 12 L/min corresponding to superficial liquor velocities of 1.1–3.3 mm/s, in the lower range of industrial values (3.0–13.6 mm/s). Axial liquor velocities were measured for three cases (Q_T/Q_B = 0.5, 1.0 and 2.0) using ERT data and compared with predictions of a CFD simulation. This data was used as input to a simple two-dimensional reaction model to predict the spatial variation of delignification through the digester.

3. Results and discussion

3.1. Accuracy and reproducibility of the ERT technique

ERT with image reconstruction using the linear back projection algorithm has allowed visualization of liquor flow in model digesters for a number of flow scenarios [2,4–6,13]. ERT gives good temporal responsiveness (sampling times as short as 0.001 s) but poor spatial resolution (only 5 to 10% of the vessel diameter) [7]. In the batch digester configuration studied here the conical section at the base of the digester presented some unique imaging challenges, although successful use of ERT for a conical geometry has

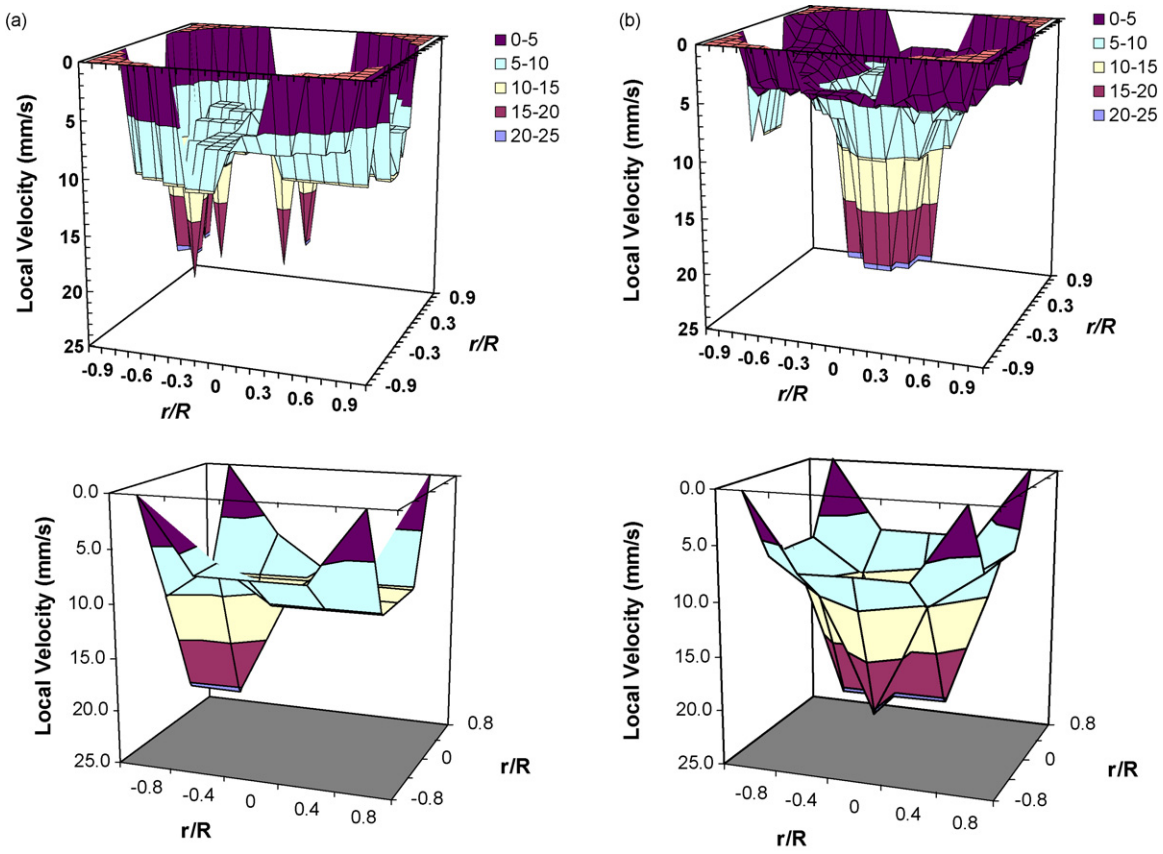

Fig. 3. Local flow velocities measured using ERT data on a pixel-by-pixel (top) and a zone-by-zone (bottom) basis for $Q_T/Q_B = 1.0$ ($Q_T = Q_B = 12$ L/min) between planes 7–8 ($z/H = 0.66$), and 5–6 ($z/H = 0.47$).

been reported [8]. The diameter of a solid rod temporarily inserted at the centre of the column and measured using ERT had the highest relative error, between 12 and 21%, in the conical section of the vessel although the contrast between the rod and fluid was most marked here. Image distortion also occurred when traced liquid flows were imaged, with the lowest sensor plane reporting spurious images caused by voltage saturation. This is likely caused by the manner used by the P2000 to set the gain map prior to data acquisition. While the effect could be minimized by the choice of background and tracer conductivities in many cases data from the lowest plane of electrodes was not used.

3.2. Formation of uniform flow zones

Fig. 2 shows the conductivity profile along the mid-plane of the vessel axis for tests in which the digester, initially filled with higher conductivity fluid (3.0 mS/cm), was displaced by a lower conductivity solution (2.5 mS/cm) added to the top left side of the vessel (as viewed). The fluid added to the bottom conical section was maintained at 3.0 mS/cm. Liquor was withdrawn uniformly from the extraction screens that ring the vessel. Three liquor splits were used: $Q_T/Q_B = 1.0$, 2.0 and 3.0 with the liquor flow in the top loop maintained at 12 L/min for all tests.

The tracer pulse moves through the top cylindrical section of the vessel slightly faster as liquor flow to the bottom of the vessel decreases (from 12 to 4 L/min). There is pronounced asymmetry to the flow, with axial flow on the right side of the vessel noticeably slower than on the left. Steady-state profiles show the establishment of symmetrical zones, with the zone of intermediate conductivity (mixed region) located lower in the vessel as Q_T/Q_B increases.

3.3. Local axial velocity measurement

Local velocities were measured using pixel cross-correlation techniques [9] for uniform (symmetric) addition of tracer to the

Table 1
Comparison of average axial velocities measured in the laboratory digester for $Q_T = Q_B = 12$ L/min.

Axial location (z/H)	Average axial velocity (mm/s)						
	Measured (ERT)				Calculated (uniform flow)	CFD (Fluent)	
	312 pixels		21 zones			Average	S.D.
	Average	S.D.	Average	S.D.			
0.66	9.1	3.0	10.3	3.6	9.3	9.3	1.6
0.47	6.3	4.9	10.7	5.7	9.3	8.0	1.6
0.28	16.4	4.8	14.2	2.3	11.3	13.5	3.4
0.18	25.7	7.8	25.9	4.1	24.7	27.9	8.3

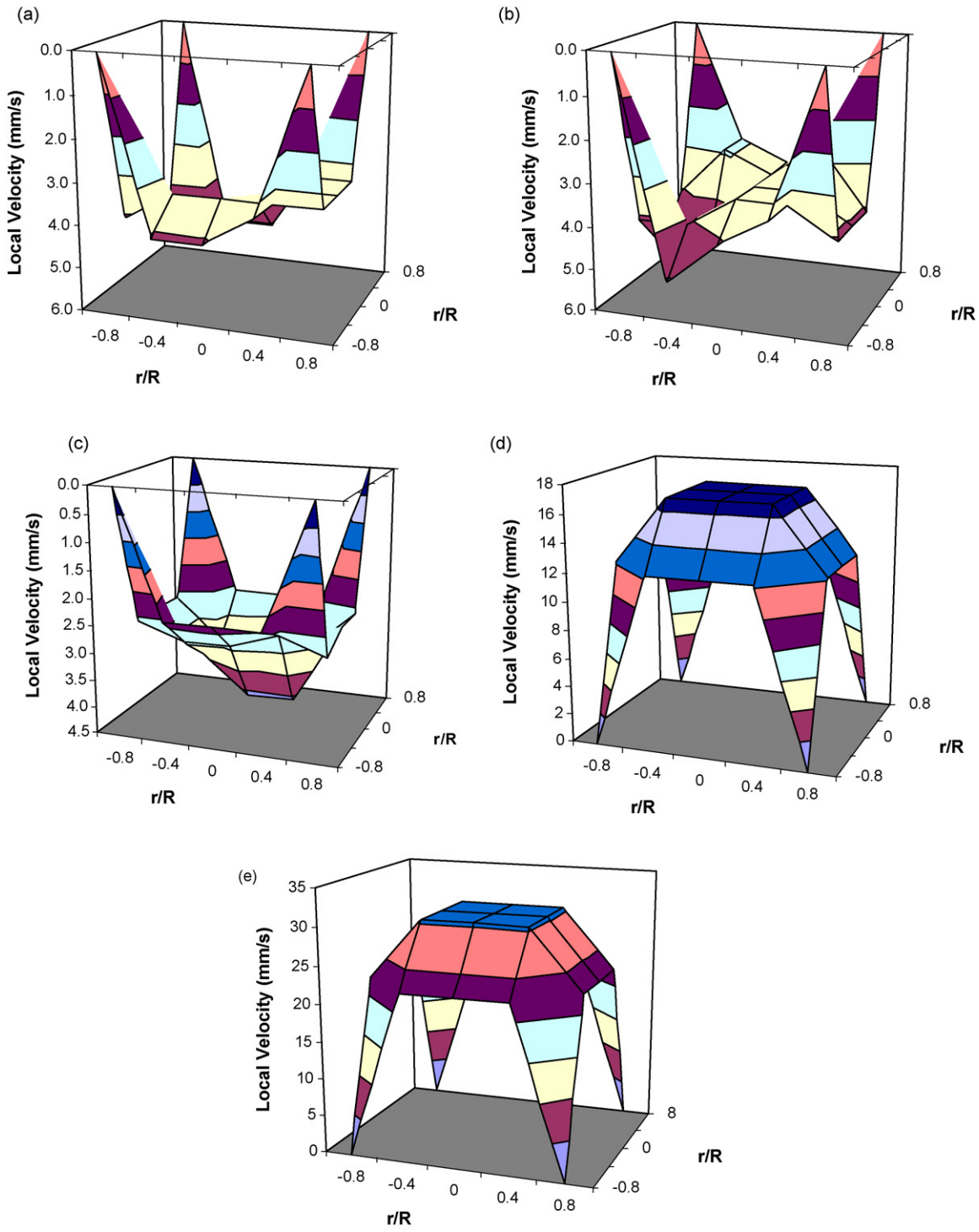

Fig. 4. Local flow velocities measured using ERT data and cross-correlation on a zone-by-zone basis for $Q_T/Q_B = 0.5$ ($Q_T = 6$ L/min; $Q_B = 12$ L/min) at z/H values of (a) 0.66, (b) 0.57, (c) 0.47, (d) 0.28 and (e) 0.18.

top and bottom of the digester. The data analysis of the technique is tedious and requires cross-correlation of tracer *vs.* time signals for axially coincident pixels on adjacent imaging planes. Two methods were used for this analysis. Method 1 used all 316 pixels in the imaging planes while method 2 grouped the data into 21 (9 interior and 16 circumferential) zones with the liquid concentration averaged in each zone prior to cross-correlation. The flow condition $Q_T = Q_B = 12$ L/min was chosen to compare both methods with the results from the two upper planes in the vessel ($z/H = 0.66$ and 0.49) shown in Fig. 3. While the radial resolution of the coarser grid is poorer, the essence of the flow profile including the asymmetry at $z/H = 0.66$ is captured. The mean velocities calculated in each plane were also similar and agreed reasonably well with the flow velocity computed assuming uniform axial flow in the plane, as shown in Table 1. Agreement is better for planes furthest from the screen section as the flow is increasingly directed radially near there. Given the significant reduction in time needed to complete analysis of a data set (a factor

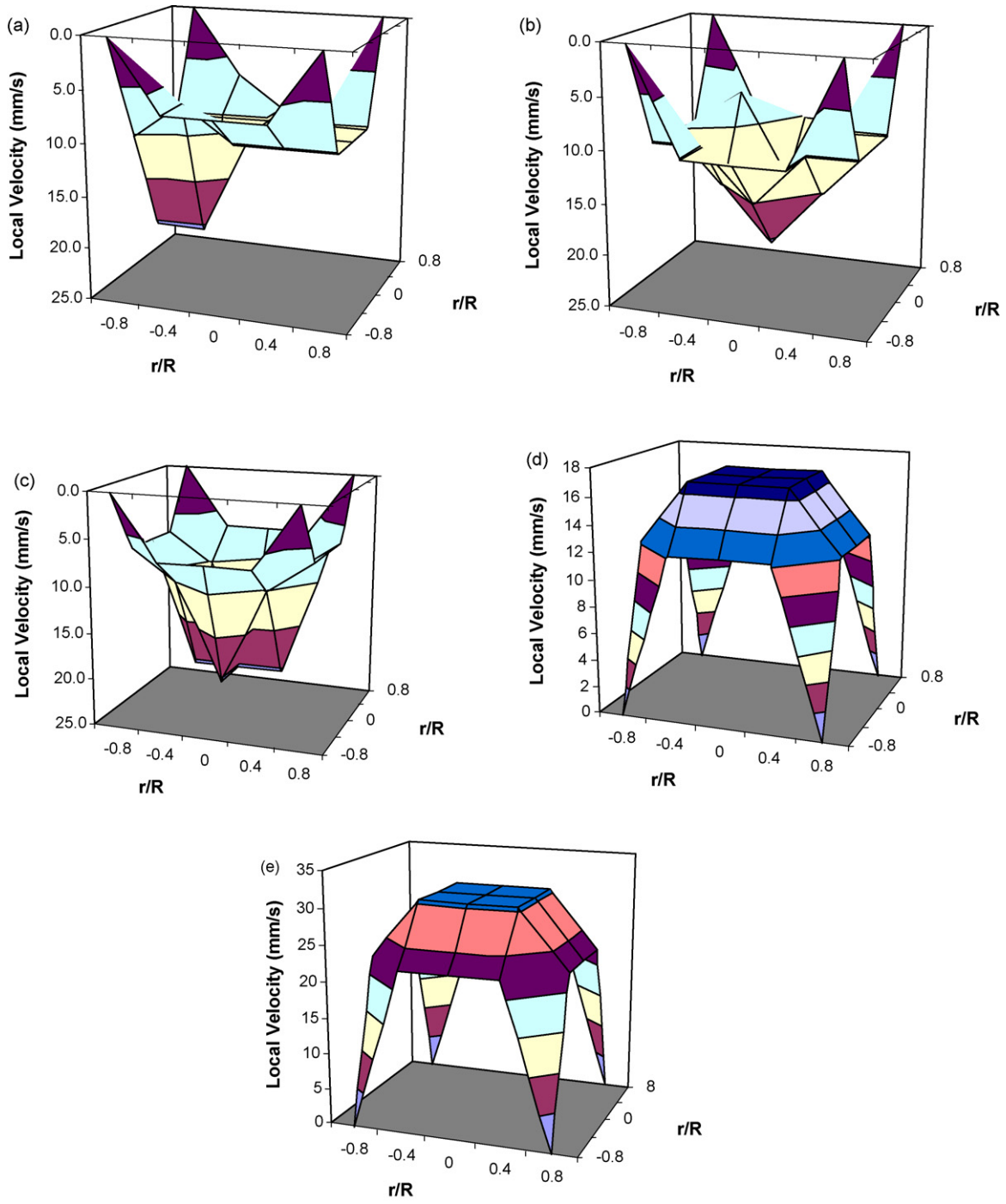

Fig. 5. Local flow velocities measured using ERT data and cross-correlation on a zone-by-zone basis for $Q_T/Q_B = 1.0$ ($Q_T = Q_B = 12$ L/min) at z/H values of (a) 0.66, (b) 0.57, (c) 0.47, (d) 0.28 and (e) 0.18.

of 312/21) the coarser grid method was used for subsequent tests.

Figs. 4–6 compare the local velocities at five axial locations in the vessel using the coarse grid for $Q_T/Q_B = 0.5$, 1.0 and 2.0. In all cases the liquid velocity and flow profile is similar when the flow rate (Q) is equivalent in the upper or lower region of the digester. Thus flow and zoning is largely segregated by the screen section of the digester. In all cases flow is not uniform across the vessel cross-section, with flow significantly reduced near the wall. This creates channeling through the centre of the vessel that is particularly evident at $z/H = 0.47$.

The accuracy of the velocity determinations was estimated using the reported spatial and temporal accuracies of the ERT measurements (spatial: ±14–28 mm; temporal ±0.15 s). This gives a theoretical error of ±19–37% over the range of velocities reported here. For an individual data point the velocity was found to be reproducible to within ±27% (although much greater accuracy was found for some tests).

A simulation of the laboratory digester was made using the commercial CFD software package Fluent v6.2 (Fluent, Inc., Lebanon, NH). The digester was assumed to be uniformly packed with incompressible solids having a uniform void fraction of 0.35. A

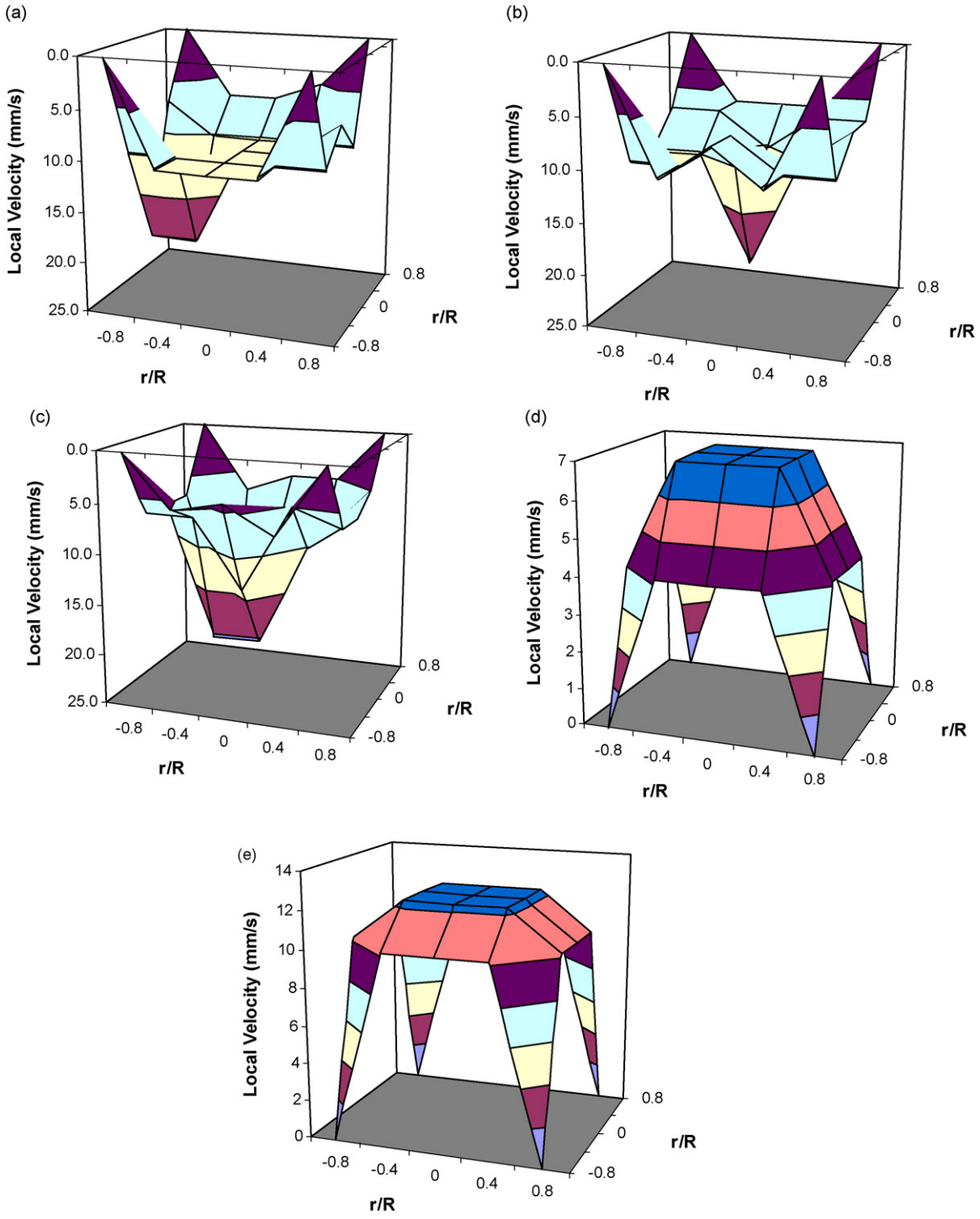

Fig. 6. Local flow velocities measured using ERT data and cross-correlation on a zone-by-zone basis for $Q_T/Q_B = 2.0$ ($Q_T = 12$ L/min; $Q_B = 6$ L/min) at z/H values of (a) 0.66, (b) 0.57, (c) 0.47, (d) 0.28 and (e) 0.18.

three-dimensional mesh of 870,000 cells was generated using Gambit software to discretize the digester volume. Uniform flow was assumed at the top and bottom liquid inlets with the screen region defined as an outflow boundary condition. The no-slip condition was applied at the vessel walls and the porous medium was assumed isotropic. The governing equations were solved using a second-order upwind scheme with calculations carried out using a 3 GHz Pentium 4 CPU with 1 GB of RAM. Iterations were continued until the scaled residuals for each transport equation were below 10^{-5}. The calculated steady-state flow field was then used to obtain the transient tracer response. A typical solution took 6–8 h. Grid and temporal independence of the solutions were checked by increasing the number of computational cells by a factor of two and reducing the discretization step size of $\Delta t = 0.1$ by a factor of ten. In both cases computed results were nearly identical.

The local axial velocities calculated with CFD are compared with the measured ERT data in Fig. 7. The ERT measurements show reasonable agreement in the lower section of the vessel but

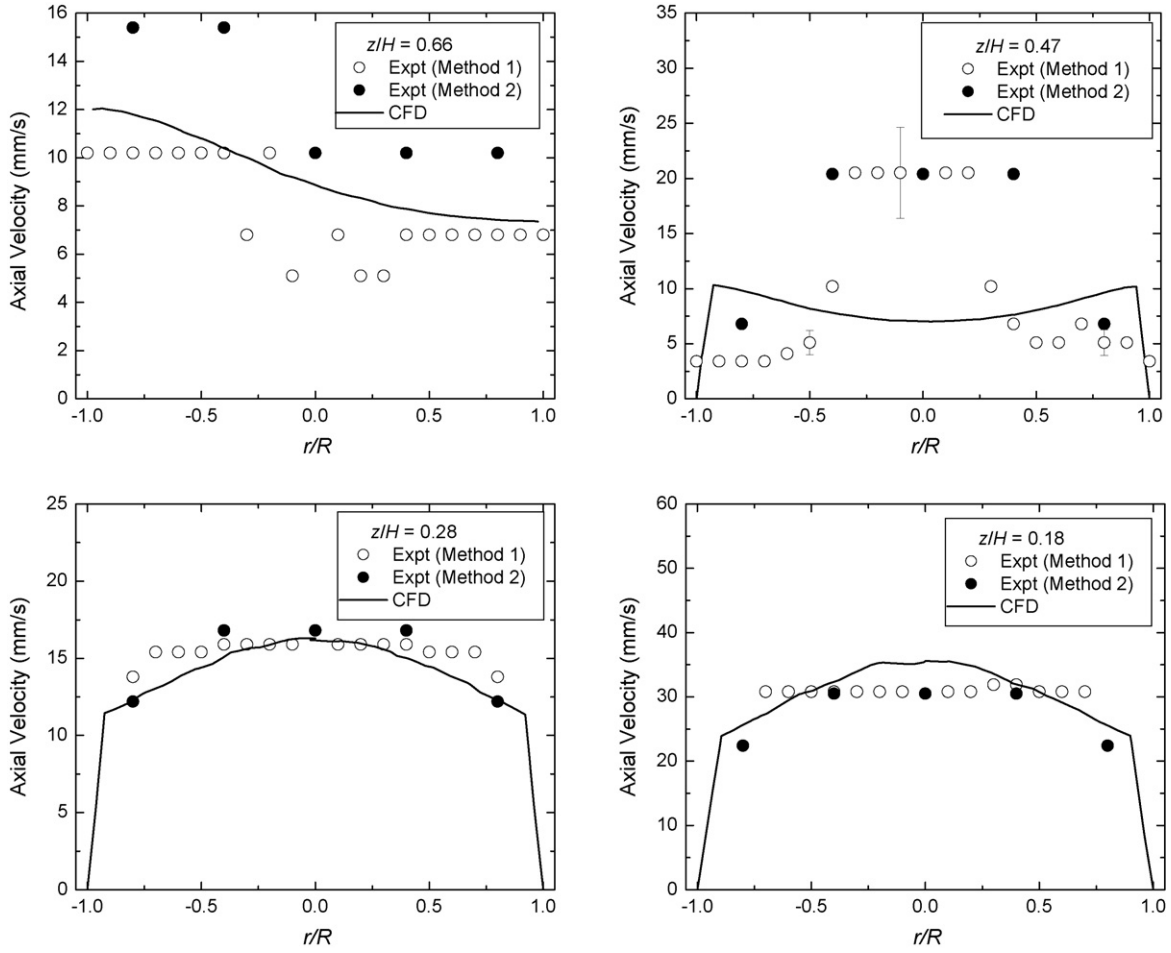

Fig. 7. Comparison of ERT measurements (experimental) and CFD simulations for $Q_T/Q_B = 1.0$ ($Q_T = Q_B = 12$ L/min) in a line (aligned with the upper feed location) through the centre of planes 7–8 and 5–6 ($D = 28$ cm), 3–4 ($D = 26.7$ cm) and 2–3 ($D = 18.8$ cm). The axial positions of the measurements are $z/H = 0.66$, 0.47, 0.28, 0.18, respectively. Method 1 uses all 316 pixels while method 2 groups each plane into 21 zones.

are significantly different above the screen section, particularly at $z/H = 0.47$ (between planes P6 and P5). At this level the ERT measures high fluid velocity at the centre of the vessel while the CFD profile is largely uniform with slightly increased flow in the near wall region (near $r/R = 0.9$). The CFD profile agrees with past work [10–12] including local velocity measurements made using ERT on a similarly configured digester (with tracer introduced isokinetically at various radial positions) [13]. The velocity profile measured here may result from the poorer accuracy of ERT at the centre of the column [14] and the 3D effect in tomographic images generated from soft-field data [15]. Apparent velocities were not resolved in the near wall region of the vessel conical section. As shown in Table 1, the average axial velocities measured by ERT and CFD vary from theoretical values (which assumes uniform axial flow) in regions of the vessel where significant radial velocity exist (in the tapered section and near the extraction screens). The ERT measurements vary from 2 to 45% of the calculated uniform values, depending on location.

Fig. 8 compares the experimental (ERT) measurements and computational (Fluent) results for the average conductivity in the plane of the extraction screens as a function of time following a step reduction in the fluid conductivity entering the top circulation loop (at $t = 0$). Three flow ratios are shown. Note that in this case the calculated tracer response (CFD) agrees well with the measured responses (ERT), particularly at $Q_T/Q_B = 0.5$ and 1.0. The calculated output for $Q_T/Q_B = 2$ is under-predicted by about 0.04 mS/cm. The discrepancy is likely due to experimental error (tracer solutions

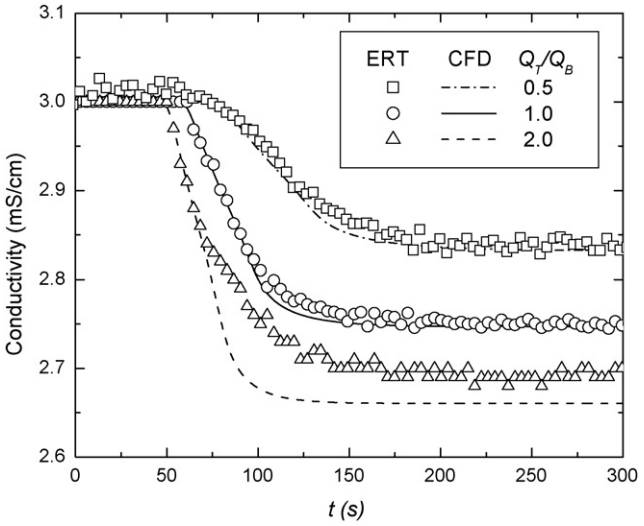

Fig. 8. Comparison of average conductivity measured in the extraction screen plane (using ERT) and simulated (using CFD). Liquor splits of $Q_T/Q_B = 0.5$, 1 and 2 with $Q_T + Q_B = 18$ L/min. A step change in conductivity (2.5 mS/cm) was introduced to the top circulation loop at $t = 0$ s. The conductivity in the lower loop was maintained at 3.0 mS/cm.

were prepared to ±0.05 mS/cm and flow rate could be measured to ±0.5 L/min) which permits the conductivity to be determined to within ±0.1 mS/cm for the test conditions.

3.4. Prediction of kappa number distribution in the digester

A two-dimensional (2D) network reaction model for a batch digester was developed, with the digester divided into 224 well-mixed cells. Delignification reaction kinetics were obtained from the literature and flow through the digester network was specified (either using the ERT measurements given here or calculated values). Detailed information on the model is available in Lee and Bennington [3].

The geometry of one industrial batch digester was modelled using typical industrial cooking conditions (temperature raised from 80 to 170 °C in a period of 1 h with the maximum temperature maintained for two additional hours). Three flow scenarios are compared here. In the first (the base case) uniform flow through the vessel was assumed (no wall effects). A total liquor flux of 0.75 m^3/(t min) (liquor flow rate per chip mass) was simulated (industrial values range from 0.69 to 0.88) with 60% of the flow circulated to the top of the digester and the balance circulated through the bottom. The lignin distribution throughout the digester following reaction is given by the kappa number, κ (the percent lignin on pulp = 0.15 × κ) [16] for the base case scenario in Fig. 9. The distribution has an average kappa number of κ = 30.6 and a CoV of 9.8%. If the liquor flux was maintained and the flow profile changed to that measured using the ERT data (assuming that the measured liquor flow rates scale geometrically to the industrial case) the breadth of the kappa distribution is increased, with κ = 34.9 and the CoV increasing to 14.9%. These increases are predominantly caused by the non-uniform liquor flow measured at the top of the laboratory vessel. If the flow profile determined using the CFD data was used κ = 31.5 and CoV = 9.8%, in better agreement with the base case examined. In industrial situations, liquor flux progressively decreases as chips become more compacted and flow resistance increases. If we also model this decreasing liquor flow with time using the base-case flow distribution the width of the kappa number distribution increases further.

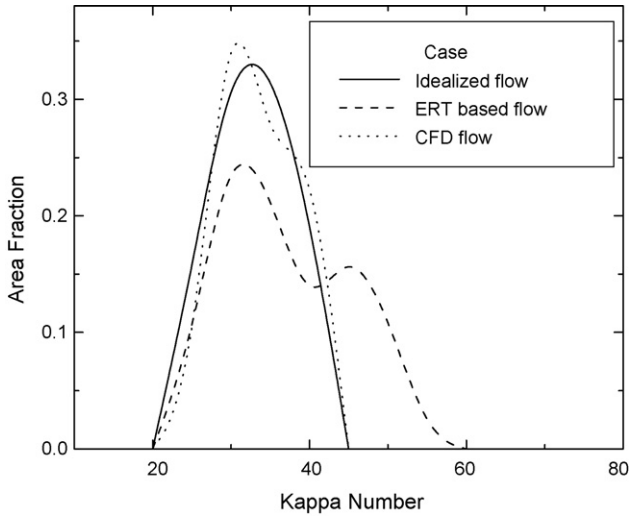

Fig. 9. Kappa number distribution predicted by a 2D reaction network model. Reaction conditions and flow scenarios as described in the text.

In Fig. 10 the spatial distribution of the kappa number through the digester is shown based on the ERT data (velocity profiles were linearly interpolated in planes not measured) (Fig. 10a and b) and the CFD computed velocity profile (Fig. 10c). Both kappa profiles are skewed above z/H = 0.6 due to non-symmetric liquor addition to the top of the vessel. The ERT-derived kappa number profile shows an unusual transition just above the screen section due to the unlikely velocity profile measured by ERT. Below the screen section the kappa number is lowest with only minor variation in kappa number calculated (for the base case, from κ = 24.2–26.6).

There is agreement between our model predictions for the location of the high kappa number regions in the digester with that reported in the literature [1]. However, the CoVs determined by the 2D model were higher than measured industrially (industrial measurements ranged from 5 to 16% and averaged 12%). The base case, which assumed ideal liquor flow, gave a CoV of 10%. Non-uniformity

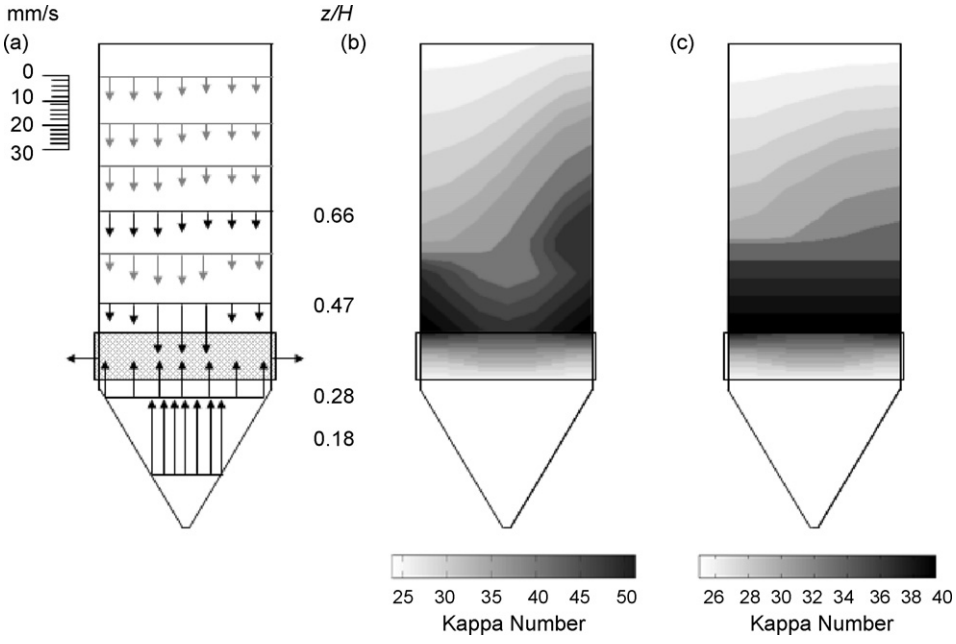

Fig. 10. (a) Flow profile used as input to the 2D reaction model (based on ERT measurements (Figs. 3 and 5)) and (b) the resulting kappa number distribution through the digester for the reaction conditions specified in the text. (c) The kappa profile calculated based on the CFD liquor velocity profile (Fig. 7) is given as comparison.

increased if the flow profile was changed or if the liquor flux was reduced during the cook. For example, combining the base case flow field with a steady reduction in liquor flux as the cook progressed (using data for a typical mill) increased the CoV to 24%. A more complete characterization of model agreement would require industrial data covering a wider range of locations in the digester.

4. Summary

ERT has been used to measure the spatial distribution of zones created by various liquor flow scenarios in a scale-model batch digester. The local velocity profile was also measured using a pixel-by-pixel cross-correlation technique. These data show that uniform zones can be created in a digester and qualitatively explain the location of high-kappa pulp measured in industrial tests. However, the accuracy of the velocity measurements is not sufficient to obtain a convincing axial liquor velocity profile in the vessel—based on a comparison with literature data and a CFD simulation of the flow field. This inaccuracy is attributed to the poor spatial resolution of the imaging technique coupled with the 3D effect that seems most pronounced at certain axial positions in the vessel. Consequently, the use of these flow fields in simulated cooks over estimates their non-uniformity. Better agreement is found with industrial data by using the flow field computed using CFD.

References

[1] M. Macleod, Basket case: kraft pulp strength variability within a batch digester, Tappi J. 73 (10) (1990) 185–190.
[2] Q.F. Lee, C.P.J. Bennington, Measuring flow velocity and uniformity using electrical resistance tomography, Can. J. Chem. Eng. 85 (1) (2007) 55–64.
[3] Q.F. Lee, C.P.J. Bennington, Kappa number distribution in batch digester operation: 2D model, J. Pulp Pap. Sci. 33 (4) (2007) 206–216.
[4] D. Vlaev, C.P.J. Bennington, Using electrical resistance tomography to image liquor flow in a model digester, J. Pulp Paper Sci. 30 (1) (2004) 15–21.
[5] D. Vlaev, C.P.J. Bennington, Flow uniformity in a model digester measured with electrical resistance tomography, Can. J. Chem. Eng. 83 (1) (2005) 42–47.
[6] D. Vlaev, C.P.J. Bennington, Flow of liquor through wood chips in a model digester, Chem. Eng. Commun. 193 (7) (2006) 879–890.
[7] R.A. Williams, M.S. Beck (Eds.), Process Tomography—Principles, Techniques and Applications, Butterworth-Heinemann, Oxford, UK, 1995.
[8] J. Bond, J.C. Cullivan, N. Climpson, R.M. Wang, R.A. Williams, Industrial monitoring of hydrocyclone operation using electrical resistance tomography, Miner. Eng. 12 (10) (1999) 1245–1252.
[9] G.T. Bolton, C.W. Hooper, R. Mann, E.H. Stitt, Flow distribution and velocity measurement in a radial flow fixed bed reactor using electrical resistance tomography, Chem. Eng. Sci. 59 (10) (2004) 1989–1997.
[10] Y. Cohen, A.B. Metzner, Wall effects in laminar flow of fluids through packed beds, AIChE J. 27 (5) (1981) 705–715.
[11] G.W. Johnson, R.S. Kapner, The dependence of axial dispersion on non-uniform flows in beds of uniform packing, Chem. Eng. Sci. 45 (11) (1990) 3329–3339.
[12] M. Song, H.F. Yin, K. Nandakumar, K.T. Chuang, A three-dimensional model for simulating the maldistribution of liquid flow in random packed beds, Can. J. Chem. Eng. 76 (2) (1998) 161–166.
[13] F. Ruzinsky, C.P.J. Bennington, Aspects of liquor flow in a model digester measured using electrical resistance tomography, Chem. Eng. J. 130 (2–3) (2007) 67–74.
[14] W.Q. Yang, J.C. Gamio, M.S. Beck, A fast iterative image reconstruction algorithm for capacitance tomography, Sens. Appl. 8 (1997) 47–52.
[15] M. Wang, Inverse solutions for electrical impedance tomography based on conjugate gradients methods, Meas. Sci. Technol. 13 (2002) 101–117.
[16] TAPPI Test Methods, Kappa number of pulp, T236-cm85, TAPPI Press, Atlanta, GA, 1996–1997.